

Accepted Article

Title: Phenanthrocarbazole-Based Dopant-Free Hole-Transport Polymer with Noncovalently Conformational Locking for Efficient Perovskite Solar Cells

Authors: Zhaoyang Yao, Yaxiao Guo, Lanlan He, Jiabin Guo, Yu Guo, Fuguo Zhang, Linqin Wang, Hao Yang, Chenhao Xiao, Yi Liu, Yongsheng Chen, and Licheng Sun

This manuscript has been accepted after peer review and appears as an Accepted Article online prior to editing, proofing, and formal publication of the final Version of Record (VoR). This work is currently citable by using the Digital Object Identifier (DOI) given below. The VoR will be published online in Early View as soon as possible and may be different to this Accepted Article as a result of editing. Readers should obtain the VoR from the journal website shown below when it is published to ensure accuracy of information. The authors are responsible for the content of this Accepted Article.

To be cited as: *Angew. Chem. Int. Ed.* 10.1002/anie.202114341

Link to VoR: <https://doi.org/10.1002/anie.202114341>

Phenanthrocarbazole-Based Dopant-Free Hole-Transport Polymer with Noncovalently Conformational Locking for Efficient Perovskite Solar Cells

Yaxiao Guo,[†] Lanlan He,[‡] Jiaxin Guo,[‡] Yu Guo,[§] Fuguo Zhang,[‡] Linqin Wang,[§] Hao Yang,[‡] Chenhao Xiao,[†] Yi Liu,^{†,*} Yongsheng Chen,[‡] Zhaoyang Yao,^{‡,*} Licheng Sun^{§,‡}

[†] State Key Laboratory of Separation Membranes and Membrane Processes, School of Chemistry, Tiangong University, Tianjin 300387, China

[‡] Key Laboratory of Functional Polymer Materials, College of Chemistry, Nankai University, Tianjin 300071, China

[‡] Department of Chemistry, KTH Royal Institute of Technology, Stockholm 10044, Sweden

[§] Center of Artificial Photosynthesis for Solar Fuels, School of Science, Westlake University, Hangzhou 310024, China

KEYWORDS: *perovskite solar cell, noncovalently conformational locking, dopant-free hole-transport polymer, phenanthrocarbazole, reorganization energy*

Accepted Manuscript

ABSTRACT: Adequate hole mobility is the prerequisite for dopant-free polymeric hole-transport materials (HTMs). Constraining configurational variation of polymer chains to afford a rigid and planar backbone can reduce unfavorable reorganization energy and improve hole mobility. Herein, a noncovalently conformational locking via S--O secondary interaction is exploited in a phenanthrocarbazole (**PC**) based polymeric HTM, **PC6**, to fix molecular geometries and significantly reduce reorganization energy. Systematic study from structurally explicit repeats to targeted polymers reveals that the broad and planar backbone of **PC** remarkably enhances π - π stacking of adjacent polymers, facilitating intermolecular charge transfer greatly. The inserted “Lewis soft” oxygen atoms passivate the trap sites efficiently at perovskite/HTM interface and further depressing interfacial recombination. Consequently, PSC employing **PC6** as dopant-free HTM offers an excellent power conversion efficiency of 22.2% and significantly improved longevity, rendering it as one of the best PSCs based on dopant-free HTMs.

Accepted Manuscript

INTRODUCTION

An amazing increase of power conversion efficiency (PCE) from 3.8% to 25.5% has been certified by perovskite solar cells (PSCs) in the last decade, which mainly benefits from the excellent light absorption and unapproachable charge-carrier transport of perovskite crystals.^[1] Despite the rapidly surging PCE, long-term stability of PSCs is another indispensable factor expediting PSCs towards economic feasibility. However, several inescapable barriers, for instance, the thermal and humidity susceptibility of perovskite crystal and interstitial degradation originating from adverse interfacial processes, still stand in the PSC's pathway to commercial application. Therefore, extensive research efforts have been made to prolong the lifespan of PSCs.^[2] In particular, special attention is drawn on the damping of PCE caused by dopants in charge transporting layers.^[3] In n-i-p type PSCs, hole-transport materials (HTMs) play an irreplaceable part in efficiently extracting and transporting holes from perovskite layer to positive electrode, besides, protecting humidity-sensitive perovskite crystals from directly confronting water in ambient atmosphere. Thus far, massive organic and inorganic materials have been developed as HTMs,^[4] among them, 2,2',7,7'-tetrakis(*N,N*-di-*p*-methoxyphenylamine)-9,9'-spirobifluorene (spiro-OMeTAD)^[5] usually acts as state-of-the-art HTM to hit record highs of PSCs.^[1g, 6] Nevertheless, the fatal weakness of spiro-OMeTAD is caused by its huge steric hindrance, resulting in an inadequate charge mobility and considerably large resistivity. That is why dopants, such as lithium bis(trifluoromethanesulfonyl)imide (LiTFSI), *tert*-butylpyridine (TBP) etc., have to be employed to improve the charge transport of spiro-OMeTAD.^[7] However, the widely applied dopants are usually featured with hygroscopicity or volatile.^[8] Moreover, the noncovalently bonded dopants can migrate and relocate in HTM layers, triggering morphology deterioration and destroying device stability.^[9] All the adverse effects mentioned above significantly spur deterioration of PSCs under practical application, rendering dopant strategy unpractical in commercial production. Thereby, massive efforts have been devoted to develop next-generation dopant-free HTMs aiming at stable and economically feasible PSCs.^[10] Thus far, very few first-class PSCs employing dopant-free HTMs have been reported.^[4f, 11]

Conjugated polymers are featured with tunable energy levels, excellent carrier mobility, good thermal stability and favorable film-forming ability, well meeting the requirements for industrial production of PSCs.^[12] Thus far, enhanced PCEs of PSCs have been achieved by dopant-free polymeric HTMs with sophisticated structures of alternately appearing donor and acceptor units.

Among them, several highly efficient systems of PBDTT^[13], PBT1-C^[14], PTEG^[15], alkoxy-PTEG (2-MA)^[16] and asy-PBTBDT,^[17] ect., have afforded over 20% PCEs. Note that poly(3-hexylthiophene) (P3HT) was also employed as polymeric HTM in a double halide architecture of PSC, demonstrating an exciting PCE over 24%.^[18] However, the applied P3HT still needs to be incorporated by gallium(III) acetylacetonate, meanwhile, a complicated interfacial treatment by *n*-hexyl trimethyl ammonium bromide is essential, jeopardizing its potential practical applications in view of either cost or reproducibility. Recently, our group developed a series of low-cost and highly efficient polymeric HTMs by replacing structurally complicated heterocyclic acceptors with thiophene analogs,^[19] indicating the rational design guideline for dopant-free polymeric HTMs. The kernels directly correlating to chemical structures include (1) two dimensionally conjugated plane to enhance intermolecular stacking, (2) hydrophobic alkyl chains to improve molecular solubility and humidity resistivity, (3) “Lewis soft” heteroatoms to passivate trap states. As we know that adequate hole mobility is the prerequisite for efficient dopant-free HTMs, while hole mobility is tightly associated with reorganization energies according to nonadiabatic semiclassical Marcus charge-transfer theory.^[20] In our guideline above, a key factor failing to take into account is the large unfavorable reorganization energy caused by considerable change of polymer geometries between ground and oxidized states. The configurational variation of polymer usually originates from semi-free rotation of adjacent aromatic rings. Therefore, how to constrain the unnecessary rotation of building blocks in polymeric HTMs is a crucial issue to further improve PCEs of PSCs. Bearing rotation constraint in mind, we designed and synthesized a phenanthrocarbazole (**PC**) based polymeric HTM **PC6** in this work. An efficient strategy of noncovalently conformational locking (S--O secondary interaction) was explored to fix molecular geometries and reduce reorganization energies. Consequently, PSC employing **PC6** as dopant-free HTM yielded an excellent PCE of 22.2% and significantly improved longevity, rendering it as one of the best PSCs based on dopant-free HTMs.

RESULTS AND DISCUSSION

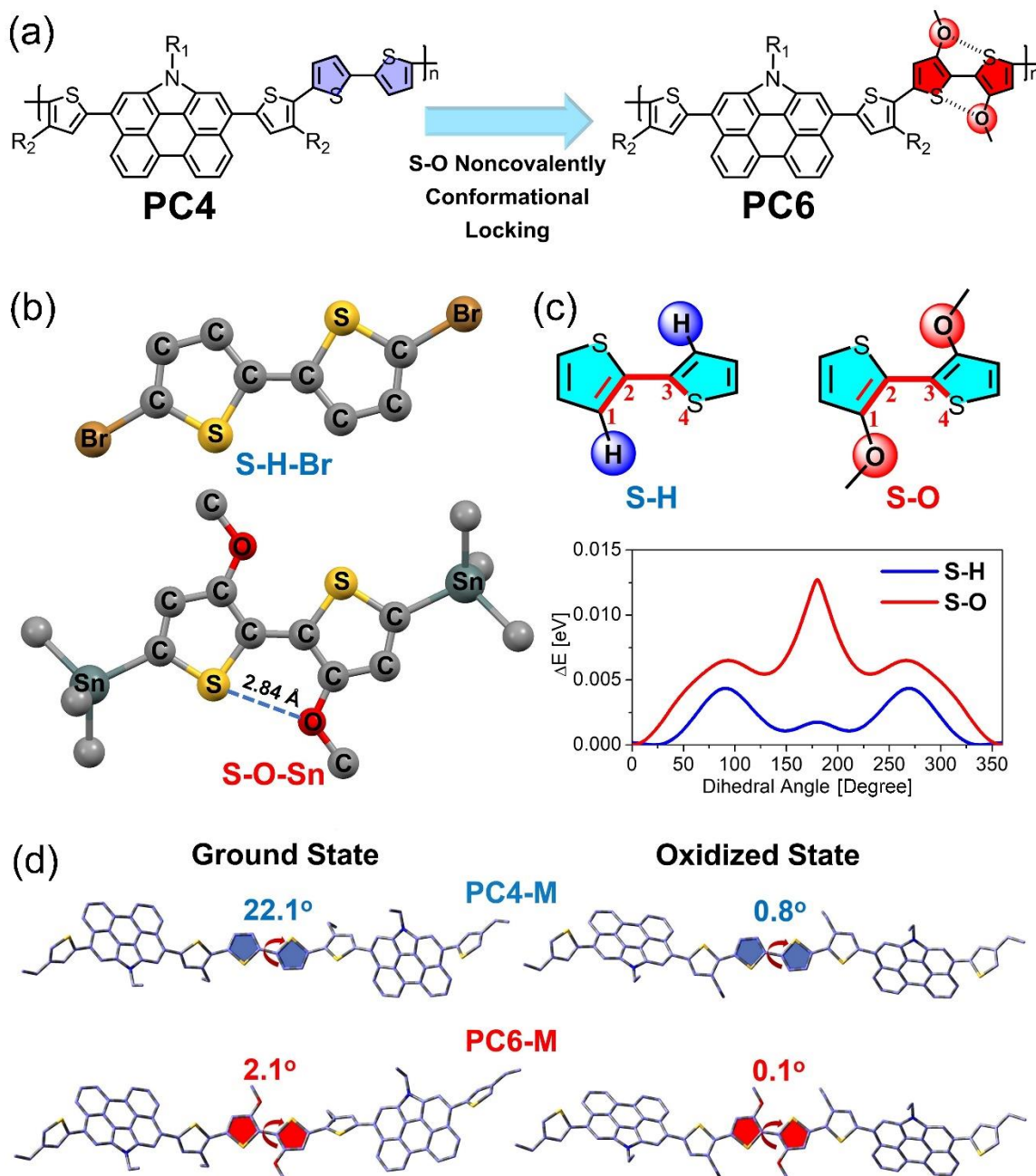


Figure 1. (a) Molecular structures of **PC4** and **PC6**. R_1 and R_2 represent 2-hexyldecane and 2-ethylhexane, respectively; (b) single crystals of bithiophene derivatives; (c) energy barriers (ΔE) of rotating dihedral angle of C1-C2-C3-S4 from 0 to 360 degrees; (d) molecular geometries of ground and oxidized states of **PC-M**. The dihedral angles between two central thiophenes were highlighted.

PC based functional molecules are usually endowed with a high luminescence yield and outstanding photostability, thus stimulating their widely applications as fluorescent lipid probes, automotive paints and photosensitizers.^[21] Herein the broad PC units were utilized as main building blocks to greatly enhance intermolecular π - π stacking between adjacent polymer strands (**Figure 1a**). Due to the strong π - π stacking, several branched aliphatic chains could be allowed to graft to improve the solubility and humidity toleration of polymers. Then thiophenes were utilized to connect PC units to maintain a relatively planar geometry. However, excessive single bond connections will cause considerably large degree of freedom of molecular geometries, resulting in unfavorable reorganization energies. Therefore, from PC4 to PC6, two oxygen atoms were selectively placed at 3,3'-positions of bithiophene, constructing a S--O noncovalently conformational locking to fix molecular geometries and reduce reorganization energies.^[22] Moreover, due to the lone pair electrons on oxygen atoms, PC6 may be able to more efficiently passivate the surface trap states caused by insufficiently coordinated lead ions compared with PC4.

In order to confirm the planar structure of alkoxy substituted bithiophene, we investigated single crystals of bithiophene analogs (**Figure S1, S2** and **Table S1** and **S2** for details). As shown in **Figure 1b**, both S-H-Br and S-O-Sn display planar geometries and the dihedral angles between two thiophene units are inclined to be zero. It is notable that the oxygen atom locates at the same side with sulfur at adjacent thiophene for S-O-Sn and the distance of sulfur to oxygen is approximate 2.84 Å, much less than the normal no-bonding van der Waals distance,^[22] in favor of successful formation of a S--O noncovalently conformational locking. In addition, the energy barriers (ΔE) of reversely rotating two thiophenes were also evaluated through density functional theory (DFT) calculations to investigate the rotation constraint. **Figure 1c** showed that S-O unit requires much more energies compared with S-H, if activating their thermodynamically stable planar configurations towards other twisted ones. Therefore, the formation of S--O noncovalently conformational locking can greatly constrain unnecessary rotation between adjacent groups and is expected to reduce reorganization energies (E_{rec}) of HTMs.^[23] In order to clearly demonstrate the change of E_{rec} , we calculated E_{rec} of PC4-M and PC6-M. **Figure 1d** showed that molecular geometries of PC4-M and PC6-M tend to be planar when transforming from ground states to oxidized states. Therefore, a planar and conformationally locked structure will suffer a smaller configurational change and result in reduced E_{rec} . As a result, PC6-M is endowed with a much

smaller E_{rec} of 0.01 eV than that of 0.21 eV for **PC4-M**, exhibiting the potential of **PC6** as an excellent dopant-free HTM.

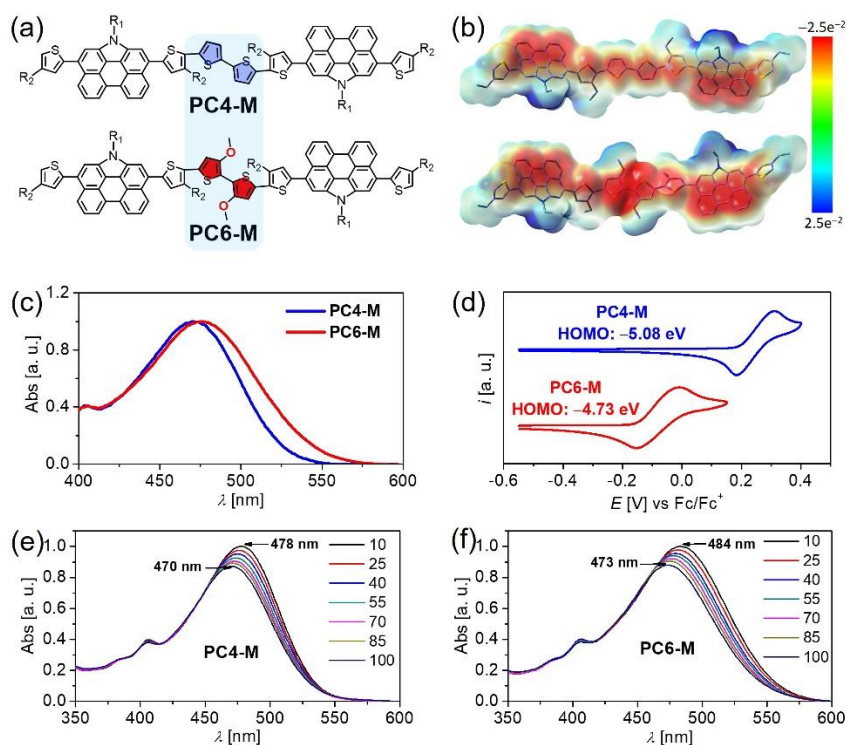


Figure 2. (a) Molecular structures of **PC4-M** and **PC6-M**; (b) optimized geometries and electrostatic surface potential maps (ESPs) obtained by DFT calculations; (c) normalized electronic absorption spectra of **PC4-M** and **PC6-M** in 20 μM THF solution; (d) cyclic voltammetry measured in solutions; (e, f) variable-temperature absorption spectra of **PC4-M** and **PC6-M** in chlorobenzene.

Diverse molecular weights may lead to much different physicochemical properties of polymeric HTMs. To exclude effects of molecular weight, we synthesized model molecules **PC4-M** and **PC6-M** with well-defined structures (**Figure 2a** and **Scheme S2**). DFT calculations in **Figure 2b** show relatively planar structures for both molecules. ESPs of **PC6-M** exhibits much more electron-rich property than that of **PC4-M**, especially around oxygen, which may facilitate the secondary interaction with coordinatively unsaturated lead (electron-withdrawing sites) at perovskite surface. The calculated highest occupied molecular orbital (HOMO) energy level of **PC6-M** is -4.59 eV, much higher than that of -4.72 eV for **PC4-M** (**Figure S3**). The greatly upshifted HOMO of **PC6-M** should be attributed to remarkably electron-donating oxygen atoms. Consequently, **PC6-M** offers a smaller energy gap of 2.57 eV with respect to 2.60 eV for **PC4-M**. It is thus plausible to

observe the red-shifted maximum absorption wavelength for **PC6-M**, regardless of in solutions or solid states (**Figure 2c** and **S4**). The experimental HOMOs were determined to be -5.08 eV for **PC4-M** and -4.73 eV for **PC6-M** (**Figure 2d**). It is worth noting that the relative alignment of energy levels is in good agreement with theoretical results (**Table S3**). Then we recorded the variable-temperature UV-*vis* spectra in chlorobenzene from 10 to 100 °C to investigate molecular stacking models (**Figure 2e** and **f**). Molecules should be most dispersed at high temperature of 100 °C, whereas intend to aggregate during cooling process, which could influence their absorption spectra.^[24] **PC6-M** exhibits more red-shifted electronic absorption peak (by 11 nm) than that of **PC4-M** (by 8 nm) from 100 to 10 °C. This tendency can be further amplified by corresponding polymers of **PC4** and **PC6** (**Figure S5a** and **S5b**), suggesting the fixed configuration by S--O conformational locking can enhance intermolecular π - π stacking of **PC6**.

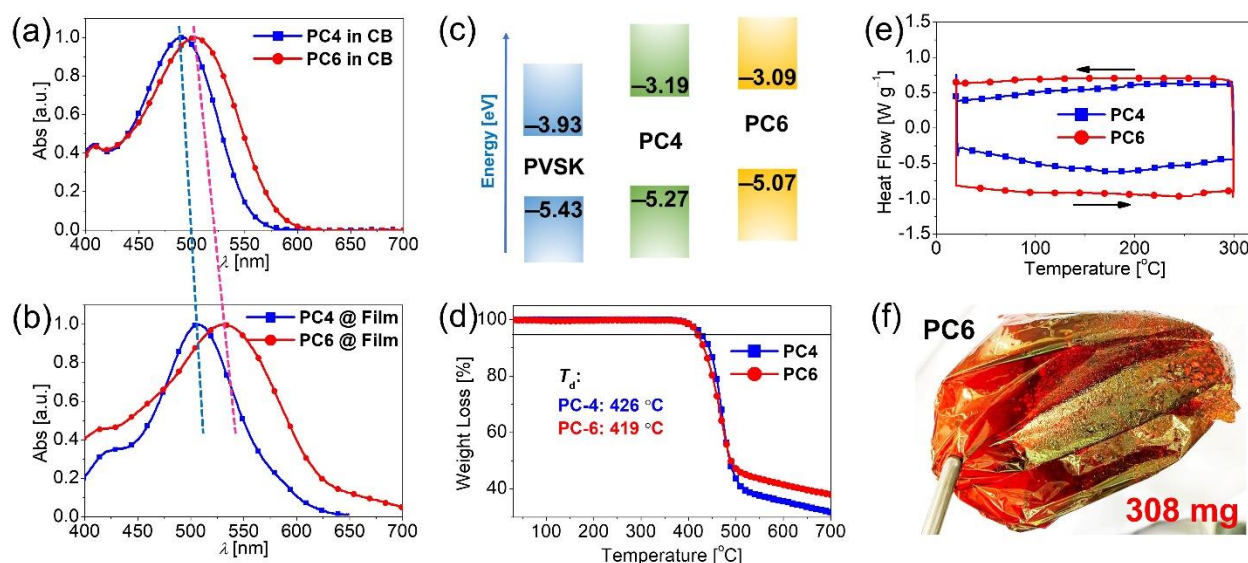


Figure 3. (a, b) Normalized electronic absorption spectra of **PC4** and **PC6** in chlorobenzene (CB) solutions and solid films; (c) energy levels of polymer films derived from CV and optical band gaps; (d) TGA traces of polymers; (e) DSC traces of polymers; (f) film of **PC6**.

The synthetic routes to polymers were illustrated in **Scheme S1**. The average molecular weights (M_n) of **PC4** and **PC6** can be estimated as 55 and 59 kDa with polydispersity indexes of 1.08 and 1.16, respectively. As shown in **Figure 3a** and **3b**, **PC6** has the maximum absorption wavelength (λ_{MAX}^{Sol}) at 501 nm, bathochromically shifted by nearly 13 nm with respect to that of 488 nm for **PC4**, which should be ascribed to the electron-donating oxygen atoms. Note that 31 nm red-shifted

maximum absorption wavelengths ($\lambda_{\text{MAX}}^{\text{Film}}$) for **PC6** can be observed from solution to solid film, larger than that of 19 nm for **PC4**, suggesting stronger π - π stacking of **PC6** induced by S--O noncovalently conformational locking.^[25] **Figure 3c** diagrammed the HOMO and LUMO energy levels derived from CVs (**Figure S5c**) and optical band gaps. The HOMOs are located at -5.27 eV for **PC4** and -5.07 eV for **PC6**, and LUMOs are determined to be -3.15 eV for **PC4** and -3.11 eV for **PC6**. The relative alignment of energy levels can well match the commonly used perovskite materials, enabling adequate driving force to extract holes from perovskite crystals and simultaneously depressing reverse electron flow to back contact. As displayed in **Figure 3d** and **3e**, the thermal gravimetric analysis (TGA) curves indicate the decomposition temperatures of 426 °C for **PC4** and 419 °C for **PC6**. Meanwhile, no obvious peak can be observed up to 300 °C according to differential scanning calorimetry (DSC), indicating no phase transition. Therefore, both polymers possess rather low crystallinity but high thermal stability, satisfying the prerequisite for durable device operation. A compact red film of **PC6** came into being due to the strong π - π stacking of **PC** backbone and fixed polymer configuration by S--O noncovalently conformational locking (**Figure 3f**). The excellent film-forming property will enable effective coverage of perovskite surface with a small amount of material. The detailed parameters associated with the physicochemical properties were listed in **Table S4**.

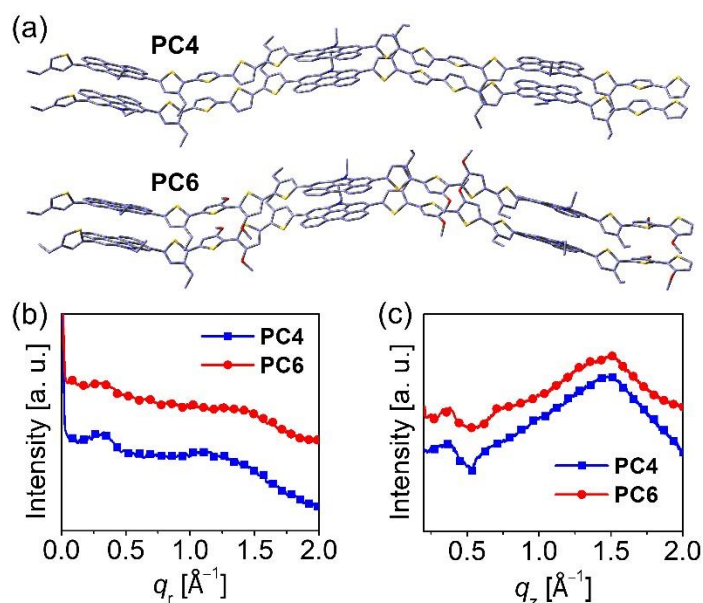


Figure 4. (a) Optimized stacking models obtained by DFT calculations; (b) in-plane, (c) out-of-plane line cuts of the 2D GIWAXS traces for two polymers on silicon substrates.

The thermostatic self-stacking models of polymers were investigated through DFT calculations by piling up two layers of each polymer segments (**Figure 4a**). As might be expected, **PC4** and **PC6** displayed the ordered molecular packing due to the highly strong intermolecular π - π interaction of **PC** units, which will undoubtedly improve the charge-transport ability of polymers. The hole mobilities (μ_h) of **PC4** and **PC6** were estimated to be 4.2×10^{-4} and 8.2×10^{-4} $\text{cm}^2 \text{V}^{-1} \text{s}^{-1}$, respectively (**Figure S6**). The higher μ_h of **PC6** should be ascribed to the stronger π - π stacking and lower reorganization energy induced by the S--O noncovalently conformational locking. In order to shed light on the intrinsic connection between μ_h and molecular packing model, grazing-incidence wide-angle X-ray scattering (GIWAXS) measurements were further performed (**Figure S7**).^[26] As recorded in **Figure 4b** and **c**, both **PC4** and **PC6** exhibited a typical face-on orientation, indicated by the apparent diffraction peaks locating at $\sim 0.29 \text{ \AA}^{-1}$ in in-plane direction and $\sim 1.5 \text{ \AA}^{-1}$ in out-of-plane direction. The favorable face-on orientation is expected to facilitate the intermolecular charge transfer of polymeric HTMs in the vertical diode architecture of PSCs. Note that **PC6** possesses a slightly smaller π - π stacking distance of $\sim 4.19 \text{ \AA}$ compared with that of 4.25 \AA for **PC4**, further verifying that noncovalently conformational locking can immobilize the geometry and give rise to a more compact packing. The closer intermolecular stacking of **PC6** will result in the more effective overlap of frontier molecular orbitals, accounting for its higher hole mobility compared to that of **PC4**.^[27] In addition, the observed larger absorption shift from solutions to thin solid films for **PC6** can be also logically explained by the enhanced molecular stacking. Generally, the favorable face-on orientation, including the more compact polymer stacking of **PC6**, is expected to output the better performance when applied as dopant-free HTM in PSCs. To further study the morphology overlaying on top of perovskite films, we carried out the atomic force microscopy (AFM) measurement. As observed in **Figure S8**, the root-mean-square (RMS) roughness of **PC4** and **PC6** were calculated to be 13.2 and 10.2 nm, respectively, greatly smaller than that of 20.9 nm for neat perovskite film. The adequate and uniform coverage of HTMs on perovskite surface can protect the perovskite layer from direct touch with moisture in the air and also with counter electrode, significantly prolonging the device durability and reducing adverse shunt losses of PSCs.

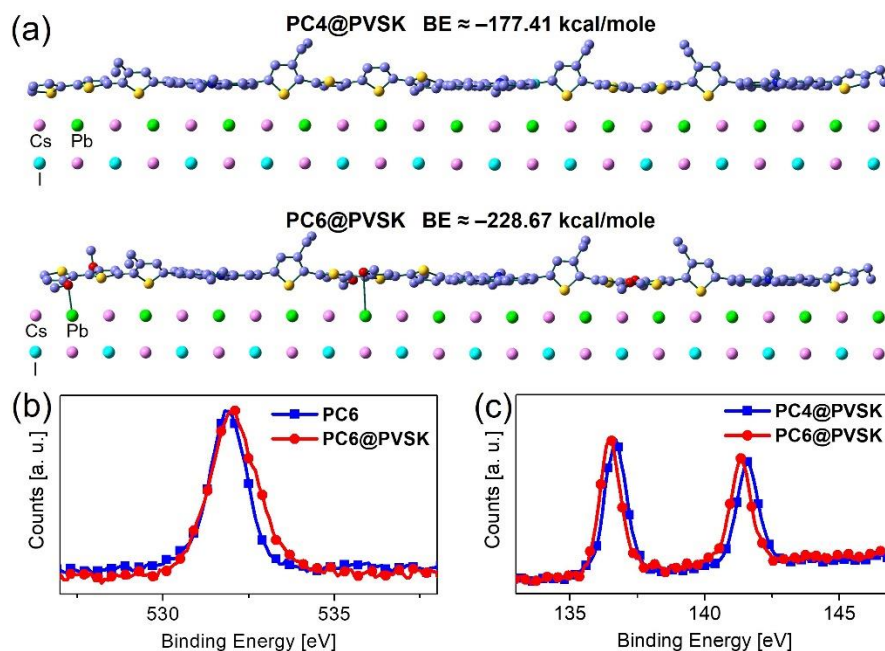


Figure 5. (a) Theoretically optimized packing of **PC** polymers and binding energies (BE) on a perovskite (PVSK) surface. The color balls of green: Pb; magenta: I; cyan: Cs; (b) XPS signals of O 2p from a pristine **PC6** film and a **PC6** coated perovskite film; (c) XPS signals of Pb 4f from **PC4**- and **PC6**-coated perovskite films.

The compact contact of HTMs with perovskite surface is indispensable for efficient hole extraction. Therefore, we implemented DFT calculations to investigate the secondary interaction between perovskite films and HTMs. As exhibited in **Figure 5a** and **Figure S9**, the structural segments of **PC4** and **PC6** with three repeat units are able to stack with perovskite surface tightly through the broad conjugated plane of **PC**. This highlights our design strategy of enhancing interfacial packing by introducing large PAH units. Note that oxygen atoms in **PC6** distribute much close to the surface of perovskite, being prone to approach lead sites and form an additional strong secondary interaction. Consequently, a prominently larger binding energy of -229 kcal/mole is achieved by **PC6** segment with respect to that of -177 kcal/mole for **PC4**. The stronger interaction between **PC6** and perovskites will result in extensive overlap of wavefunction at perovskite/HTM interface and hence facilitate hole extraction. To further clarify the effect of oxygen passivation, we carried out the X-ray photoelectron spectroscopy (XPS) to monitor the binding energy variation of characteristic peaks of O 2p and Pb 4f orbitals. The O 2p peak of **PC6**-capped perovskite films emerges at 532.1 eV, slightly larger than that of 531.8 eV for a pristine **PC6** film (**Figure 5b**),

suggesting an efficient interaction between oxygen atoms and perovskite surface. Furthermore, as displayed in **Figure 5c**, the symmetric peaks of **PC4**-coated perovskite films locate at 136.7 and 141.5 eV, corresponding to Pb 4f core level. A ~ 4.8 eV gap of spin-orbit split between 4f_{7/2} and 4f_{5/2} can be observed, in good agreement with the literature values.^[28] Note that the characteristic peaks of Pb for **PC6**-coated perovskite films appears at 136.5 eV and 141.3 eV. The ~ 0.2 eV displacement towards the low-binding energy region from **PC4** to **PC6** should be ascribed to the potential Pb–O interaction. Given that the amount of surface trap states can partially indicate the extent of passivation by HTMs, we further measured trap-state densities of **PC4** and **PC6** coated perovskite films, being $1.19 \times 10^{16} \text{ cm}^{-3}$ for **PC4** and $9.28 \times 10^{15} \text{ cm}^{-3}$ for **PC6** (**Figure S10**). The prominently reduced trap-state density of **PC6** can be ascribed to the additional passivation effect of oxygen, which is in good accordance with the discussions above. The lower trap states density is expected to yield fewer recombination sites and thus contributes to an improved photovoltaic performance.

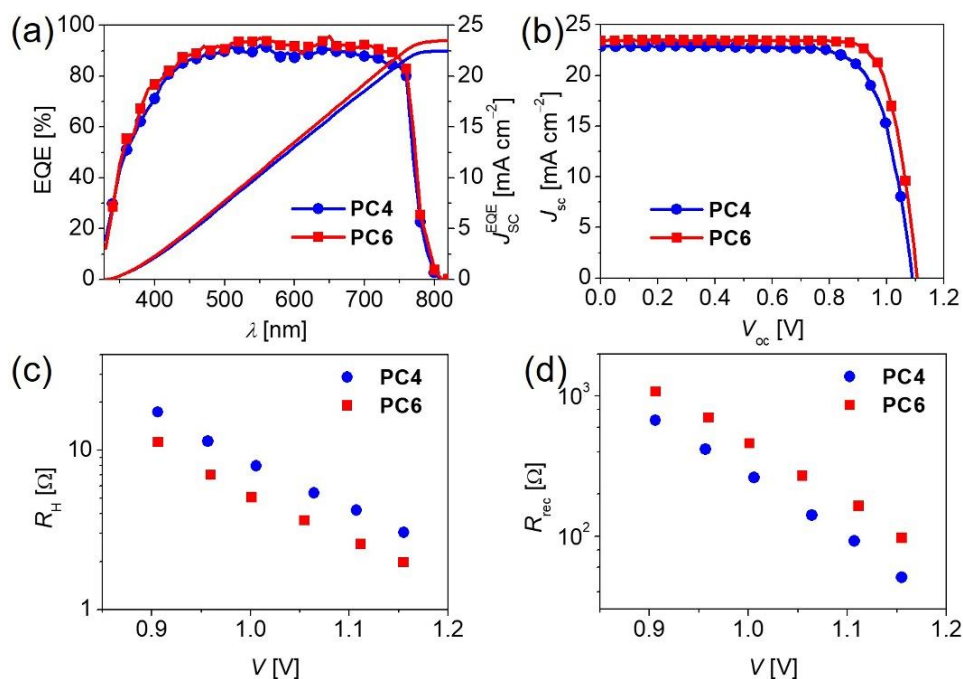


Figure 6. (a) EQEs and J_{sc}^{EQE} derived from the **PC4** and **PC6** based PSCs; (b) J – V curves; (c) bias voltage dependent hole transport resistance of PSCs; (d) bias voltage dependent interface recombination resistance of PSCs.

To evaluate the interfacial charge transfer, time-resolved PL decay (TRPL) traces were recorded in **Figure S11**. The significantly PL quenching occurs when coating two HTMs on top of perovskite films, suggesting efficient hole extraction at the energy-offset perovskite/HTM interface. Moreover, **PC6** capped perovskite film displayed an obviously reduced PL lifetime as compared to **PC4** (**Table S5**), indicating a more efficient hole extraction from perovskite. The higher HOMO and stronger interfacial interaction with perovskite films for **PC6** should account for the enhanced hole extraction and transport. Then PSCs with a structure of glass/FTO/SnO₂/perovskite (MAPbI₃)/HTM/Au were fabricated to evaluate the potential of **PC4** and **PC6** as dopant-free HTMs. HTM film thickness related performance was firstly investigated and both HTMs contributed to the best device with a low precursor concentration of ~5 mg/mL (**Figure S12** and **Table S6**). The concentration is markedly smaller than that of spiro-OMeTAD (>80 mg/mL), in favor of enhancing economic feasibility of PSCs. As displayed in **Figure 6a**, both PSCs exhibited excellent external quantum efficiencies (EQEs) with integrated current densities (J_{sc}^{EQE}) of 22.5 and 23.3 mA·cm⁻² for **PC4** and **PC6**, respectively. **Figure 6b** displayed that PSCs employing **PC4** as the dopant-free HTM offered a good PCE of 18.9% accompanied by a J_{sc} of 22.8 mA·cm⁻², a V_{oc} of 1.09 V and an FF of 76.2%. In contrast, after configurational locking by S-O secondary interaction, **PC6** based PSCs output a much better PCE of 21.0% and entirely upgraded J_{sc} , V_{oc} and FF, being 23.5 mA·cm⁻², 1.11 V and 80.3%, respectively (**Table 1**). The negligible hysteresis effects, superior and highly stable PCEs recorded at the maximum power point (MPP) qualify **PC6** based PSCs as one of the best devices using dopant-free HTMs (**Figure S13~S15**). Note that a higher V_{oc} of 1.11 V was afforded by **PC6** based PSCs with respect to that of 1.09 V for **PC4**, despite the upshifted HOMO of **PC6**. We further implemented the electrochemical impedance spectroscopy (EIS) to reveal the origin of V_{oc} and FF improvement. Two kernel parameters are involved, R_H and R_{rec} ,^[29] among them, R_H and R_{rec} act as the charge transport resistance and recombination resistance of HTMs layer, respectively. As shown in **Figure 6c**, PSCs based on **PC6** possess a lower R_H at a given bias voltage with respect to that of **PC4**, which can be attributed to its increased hole mobility. Meanwhile, an enlarged R_{rec} alternating from **PC4** to **PC6** can be recorded (**Figure 6d**), demonstrating a depressed interfacial charge recombination for **PC6** based PSCs. Generally, the larger R_{rec} originates from more efficient

interfacial passivation caused by additional Pb-O secondary interaction, while the smaller R_h is evoked by multiple factors such as fixed molecular geometry, strong intermolecular interaction and also efficiently stacking with perovskite. The efficient interfacial passivation of **PC6** based PSCs results in large interface recombination resistance and small hole transport resistance, which should account for its higher V_{oc} with respect to that of **PC4**. Besides, the enlarged hole mobility of **PC6** and enhanced π - π stacking with perovskite surface should account for the improved FF. The statistical analysis for each polymer and also three different batches of **PC6** demonstrates an excellent synthetic and device reproducibility for **PC6** (Figure S16 and S17). This extricated **PC6** based PSCs from susceptible device preparation, which is meaningful for large-scale production.

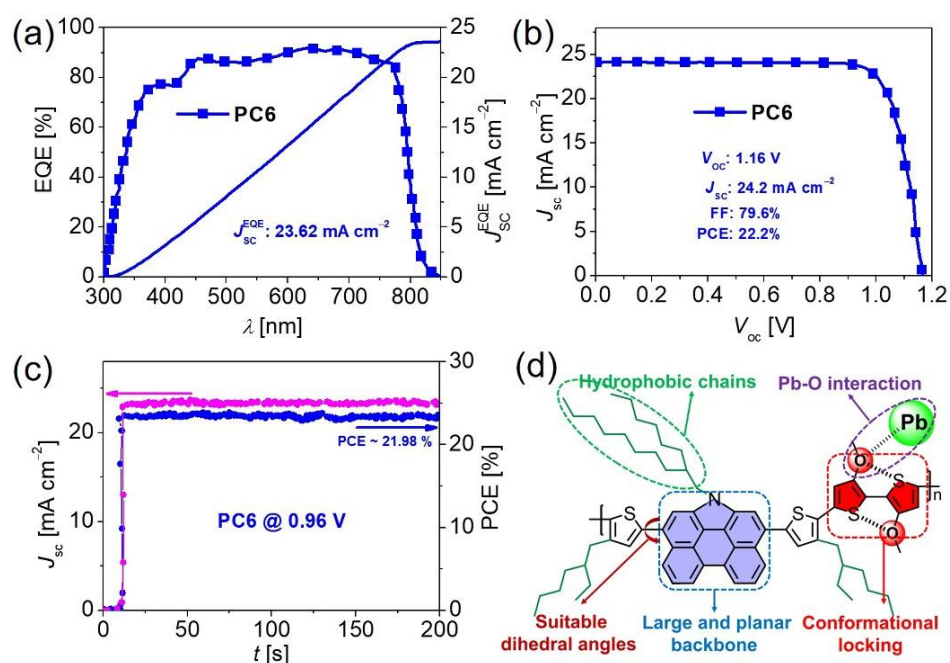


Figure 7. (a) EQEs and J_{sc}^{EQE} derived from **PC6** based PSC; (b) J - V curves; (c) steady-state output of photocurrent density and PCE; (d) Structure-function relation analysis of **PC6** HTM.

In view of the huge potential of **PC6** as efficient dopant-free HTM, we further explored its application in PSCs with an architecture of glass/ITO/SnO₂/perovskite (FA_{0.85}MA_{0.15}PbI₃)/HTM/MoO₃/Ag. With the aid of post-passivation^[30], the resulting PSCs can offer better V_{oc} and J_{sc} due to the broader absorption range and less recombination sites of mixed perovskite crystals. Consequently, PSCs employing **PC6** as the dopant-free HTM afford an excellent J_{sc} of 24.2 $\text{mA}\cdot\text{cm}^{-2}$, V_{oc} of 1.16 V and an FF of 79.6%, generating an impressive

22.2% PCE which ranks in the best PSCs using dopant-free HTMs according to our knowledge (**Figure 7b**). The integrated J_{SC}^{EQE} derived from EQE spectrum in **Figure 7a** was estimated to be 23.9 mA cm⁻², being in good agreement with $J-V$ characters. Moreover, the steady-state power output at MPP was recorded for 200 s, displaying a steady efficiency of 21.96% (**Figure 7c**). Note that the **PC6**-based PSCs also displayed a superior device reproducibility (**Figure S18**), rendering **PC6** as an efficient and feasible HTM candidate for the potential large-scale production of PSCs.

Table 1. Photovoltaic Parameters of PSCs Based on Dopant-Free Polymeric HTMs and Doped Spiro-OMeTAD.

HTMs	J_{SC}^{EQE} [mA cm ⁻²]	J_{SC} [mA cm ⁻²]	V_{oc} [V]	FF [%]	PCE [%]
PC4	22.5	22.8	1.09	76.2	18.9
PC6	23.3	23.5	1.11	80.3	21.0
PC6^a	23.9	24.2	1.16	79.6	22.2
Spiro-OMeTAD	23.1	23.2	1.10	79.8	20.4 (Doped)

^a Device parameters of PSCs using mixed perovskite.

Humidity-induced decomposition of perovskite crystals is a vital degradation pathway for PSCs. Therefore, sufficient hydrophobic alkyl chains are usually needed to improve the water-repelling properties of HTMs capped perovskite films. However, bulky alkyl chains may impede the effective interactions between neighboring polymer strands and also with perovskite films, hence hindering efficient charge transfer. Herein, a delicate balance between enough humidity resistivity and highly strong intermolecular or interfacial interaction was established in **PC6** owing to the broad **PC** plane as well as noncovalently conformational locking. Quite large contact angles of ~100° was observed when placing a water droplet on **PC** polymer layers, much larger than ~60° on neat perovskite films (**Figure S19**). This demonstrates an effective protection of the hygroscopic perovskite crystals from water molecules in ambient atmosphere. It is thus plausible to observe our champion PSCs employing **PC6** as dopant-free HTM exhibit much improved long-term stability under ambient atmosphere with respect to that of doped spiro-OMeTAD (**Figure S20a**). After a fast initial burn-in decay,^[4d] **PC6** based PSCs still possessed an excellent PCE when placed under the irradiation of continuous AM1.5 G equivalent light at 40 °C for 1000 h. In contrary, a nearly >80% PCE loss could be observed for doped spiro-OMeTAD based PSCs

(**Figure S20b**) because of the definitely hygroscopic property of applied dopants in spiro-OMeTAD. Generally, **PC6** as dopant-free HTM features the remarkable ability to produce PSCs with both high efficiency and excellent durability.

Besides several well-known prerequisites, such as suitable energy levels, high hole mobilities and excellent stabilities, a comprehensive image was depicted to demonstrate the essential architectural features of efficient dopant-free HTMs, being (1) two dimensionally planar conjugated backbones to achieve strong intermolecular π - π stacking and compact packing with perovskite; (2) suitable dihedral angles to improve hole mobilities on the premise of adequate solubilities; (3) enough hydrophobic aliphatic chains to improve humidity resistivity of PSCs; (4) several “Lewis soft” atoms to passivate coordinatively unsaturated lead ions on perovskite surface; (5) fixed molecular configurations by use of noncovalent secondary interactions to reduce recombination energies (**Figure 7d**).

CONCLUSION

In summary, an efficient strategy of noncovalently conformational locking via S--O secondary interaction in a **PC** based polymeric HTM is successfully exploited to fix the molecular geometries, reduce the reorganization energy and further improve the PCE of dopant-free HTM based PSCs. Systematic study from the structurally explicit repeat segments (**PC4-M** and **PC6-M**) to targeted polymers (**PC4** and **PC6**) reveals that the broad and planar **PC** unit can greatly enhanced the intermolecular π - π stacking of polymers, as well as compact packing with the perovskite surface. The introduced “Lewis soft” oxygen atoms are able to efficiently passivate the coordinatively unsaturated lead ions at perovskite/HTM interface, suppressing the interfacial recombination and enlarging the V_{oc} of PSCs. As a result, the PSCs using multifunctional **PC6** as dopant-free HTM, yield an excellent PCE of 22.2% and significantly improved longevity. The combined excellent PCE and stability qualify **PC6** as an encouraging dopant-free HTM for commercially feasible PSCs. This work developed a semiempirical design principle for dopant-free polymeric HTMs and will inspire the rational exploration of dopant-free polymeric, even small molecular HTMs.

ASSOCIATED CONTENT

Supporting Information. The detailed experimental methods, including material synthesis and device preparation were described. The additional figures, tables and spectra were also listed. The involved CIFs of single crystal were deposited in CCDC (2116919 and 2116920).

AUTHOR INFORMATION

Corresponding Author

* E-mail: zyao@nankai.edu.cn

* E-mail: yiliuchem@whu.edu.cn

Conflict of interest

The authors declare no competing financial interest.

ACKNOWLEDGMENT

This work was financially supported by the 100 Young Academic Leaders Program of Nankai University (Grants No. 020-63213096) and MoST (2019YFA0705900 of China).

REFERENCES

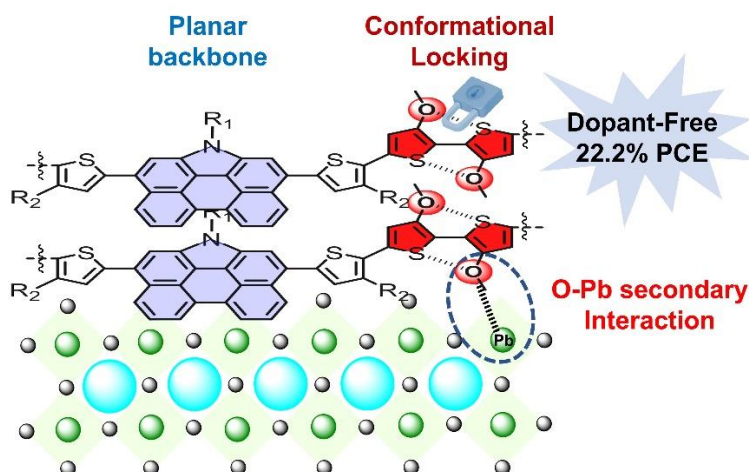
- [1] a) A. Kojima, K. Teshima, Y. Shirai, T. Miyasaka, *J. Am. Chem. Soc.* **2009**, *131*, 6050–6051; b) H.-S. Kim, C.-R. Lee, J.-H. Im, K.-B. Lee, T. Moehl, A. Marchioro, S.-J. Moon, R. Humphry-Baker, J.-H. Yum, J. E. Moser, M. Grätzel, N.-G. Park, *Sci. Rep.* **2012**, *2*, 591; c) Q. Dong, Y. Fang, Y. Shao, P. Mulligan, J. Qiu, L. Cao, J. Huang, *Science* **2015**, *347*, 967–970; d) C. Eames, J. M. Frost, P. R. F. Barnes, B. C. O'Regan, A. Walsh, M. S. Islam, *Nat. Commun.* **2015**, *6*, 7497; e) W. S. Yang, B.-W. Park, E. H. Jung, N. J. Jeon, Y. C. Kim, D. U. Lee, S. S. Shin, J. Seo, E. K. Kim, J. H. Noh, S. I. Seok, *Science* **2017**, *356*, 1376–1379; f) E. H. Jung, N. J. Jeon, E. Y. Park, C. S. Moon, T. J. Shin, T.-Y. Yang, J. H. Noh, J. Seo, *Nature* **2019**, *567*, 511–515; g) Q. Jiang, Y. Zhao, X. Zhang, X. Yang, Y. Chen, Z. Chu, Q. Ye, X. Li, Z. Yin, J. You, *Nat. Photonics* **2019**, *13*, 460–466; h) NREL; i) Q. Wang, N. Phung, D. Di Girolamo, P. Vivo, A. Abate, *Energy Environ. Sci.* **2019**, *12*, 865–886.
- [2] a) N.-G. Park, M. Grätzel, T. Miyasaka, K. Zhu, K. Emery, *Nat. Energy* **2016**, *1*, 16152; b) B. Roose, Q. Wang, A. Abate, *Adv. Energy Mater.* **2019**, *9*, 1803140; c) T.-H. Han, S. Tan,

- J. Xue, L. Meng, J.-W. Lee, Y. Yang, *Adv. Mater.* **2019**, *31*, 1803515; d) A. Uddin, M. B. Upama, H. Yi, L. Duan, *Coatings* **2019**, *9*, 65.
- [3] A. K. Jena, A. Kulkarni, T. Miyasaka, *Chem. Rev.* **2019**, *119*, 3036–3103.
- [4] a) M. Saliba, S. Orlandi, T. Matsui, S. Aghazada, M. Cavazzini, J.-P. Correa-Baena, P. Gao, R. Scopelliti, E. Mosconi, K.-H. Dahmen, F. De Angelis, A. Abate, A. Hagfeldt, G. Pozzi, M. Graetzel, M. K. Nazeeruddin, *Nat. Energy* **2016**, *1*, 15017; b) Q.-Q. Ge, J.-Y. Shao, J. Ding, L.-Y. Deng, W.-K. Zhou, Y.-X. Chen, J.-Y. Ma, L.-J. Wan, J. Yao, J.-S. Hu, Y.-W. Zhong, *Angew. Chem., Int. Ed.* **2018**, *57*, 10959–10965; *Angew. Chem.*, **2018**, *130*, 11125–11131; c) V. A. Chiykowski, Y. Cao, H. Tan, D. P. Tabor, E. H. Sargent, A. Aspuru-Guzik, C. P. Berlinguette, *Angew. Chem., Int. Ed.* **2018**, *57*, 15529–15533; *Angew. Chem.*, **2018**, *130*, 15755–15759; d) J. A. Christians, P. Schulz, J. S. Tinkham, T. H. Schloemer, S. P. Harvey, B. J. Tremolet de Villers, A. Sellinger, J. J. Berry, J. M. Luther, *Nat. Energy* **2018**, *3*, 68–74; e) C. Shen, Y. Wu, H. Zhang, E. Li, W. Zhang, X. Xu, W. Wu, H. Tian, W.-H. Zhu, *Angew. Chem., Int. Ed.* **2019**, *58*, 3784–3789; *Angew. Chem.*, **2019**, *131*, 3824–3829; f) N. Cai, F. Li, Y. Chen, R. Luo, T. Hu, F. Lin, S.-M. Yiu, D. Liu, D. Lei, Z. Zhu, A. K.-Y. Jen, *Angew. Chem., Int. Ed.* **2021**, *60*, 20437–20442; *Angew. Chem.*, **2021**, *133*, 20600–20605.
- [5] J. Salbeck, N. Yu, J. Bauer, F. Weissörtel, H. Bestgen, *Synth. Met.* **1997**, *91*, 209–215.
- [6] M. Kim, G.-H. Kim, T. K. Lee, I. W. Choi, H. W. Choi, Y. Jo, Y. J. Yoon, J. W. Kim, J. Lee, D. Huh, H. Lee, S. K. Kwak, J. Y. Kim, D. S. Kim, *Joule* **2019**, *3*, 2179–2192.
- [7] a) J. Burschka, A. Dualeh, F. Kessler, E. Baranoff, N.-L. Cevey-Ha, C. Yi, M. K. Nazeeruddin, M. Grätzel, *J. Am. Chem. Soc.* **2011**, *133*, 18042–18045; b) T. Leijtens, J. Lim, J. Teuscher, T. Park, H. J. Snaith, *Adv. Mater.* **2013**, *25*, 3227–3233.
- [8] a) F. Fabregat-Santiago, J. Bisquert, L. Cevey, P. Chen, M. Wang, S. M. Zakeeruddin, M. Grätzel, *J. Am. Chem. Soc.* **2009**, *131*, 558–562; b) J. Liu, Y. Wu, C. Qin, X. Yang, T. Yasuda, A. Islam, K. Zhang, W. Peng, W. Chen, L. Han, *Energy Environ. Sci.* **2014**, *7*, 2963–2967.
- [9] a) A. K. Jena, M. Ikegami, T. Miyasaka, *ACS Energy Lett.* **2017**, *2*, 1760–1761; b) G. Parthasarathy, C. Shen, A. Kahn, S. R. Forrest, *J. Appl. Phys.* **2001**, *89*, 4986–4992; c) E.

- J. Juarez-Perez, M. R. Leyden, S. Wang, L. K. Ono, Z. Hawash, Y. Qi, *Chem. Mater.* **2016**, *28*, 5702–5709.
- [10] a) K. Rakstys, S. Paek, P. Gao, P. Gratia, T. Marszalek, G. Grancini, K. T. Cho, K. Genevicius, V. Jankauskas, W. Pisula, M. K. Nazeeruddin, *J. Mater. Chem. A* **2017**, *5*, 7811–7815; b) B. Xu, D. Bi, Y. Hua, P. Liu, M. Cheng, M. Grätzel, L. Kloo, A. Hagfeldt, L. Sun, *Energy Environ. Sci.* **2016**, *9*, 873–877; c) W. Zhou, Z. Wen, P. Gao, *Adv. Energy Mater.* **2018**, *8*, 1702512.
- [11] H. Guo, H. Zhang, C. Shen, D. Zhang, S. Liu, Y. Wu, W.-H. Zhu, *Angew. Chem., Int. Ed.* **2021**, *60*, 2674–2679; *Angew. Chem.*, **2021**, *133*, 2706–2711.
- [12] a) W. Hou, Y. Xiao, G. Han, J.-Y. Lin, *Polymers* **2019**, *11*, 143; b) M. Al-Hussein, E. M. Herzig, M. Schindler, F. Löhner, C. M. Palumbiny, W. Wang, S. V. Roth, P. Müller-Buschbaum, *Polym. Eng. Sci.* **2016**, *56*, 889–894; c) Y. Zhang, Y. Ren, X. Xie, Y. Wei, L. He, L. Fang, J. Zhang, Y. Yuan, P. Wang, *Adv. Funct. Mater.*, *n/a*, 2108855.
- [13] G. You, Q. Zhuang, L. Wang, X. Lin, D. Zou, Z. Lin, H. Zhen, W. Zhuang, Q. Ling, *Adv. Energy Mater.* **2020**, *10*, 1903146.
- [14] F. Qi, X. Deng, X. Wu, L. Huo, Y. Xiao, X. Lu, Z. Zhu, A. K.-Y. Jen, *Adv. Energy Mater.* **2019**, *9*, 1902600.
- [15] G.-W. Kim, J. Lee, G. Kang, T. Kim, T. Park, *Adv. Energy Mater.* **2018**, *8*, 1701935.
- [16] J. Lee, G.-W. Kim, M. Kim, S. A. Park, T. Park, *Adv. Energy Mater.* **2020**, *10*, 1902662.
- [17] J. Lee, M. Malekshahi Byranvand, G. Kang, S. Y. Son, S. Song, G.-W. Kim, T. Park, *J. Am. Chem. Soc.* **2017**, *139*, 12175–12181.
- [18] M. J. Jeong, K. M. Yeom, S. J. Kim, E. H. Jung, J. H. Noh, *Energy Environ. Sci.* **2021**, *14*, 2419–2428.
- [19] Z. Yao, F. Zhang, Y. Guo, H. Wu, L. He, Z. Liu, B. Cai, Y. Guo, C. J. Brett, Y. Li, C. V. Srambickal, X. Yang, G. Chen, J. Widengren, D. Liu, J. M. Gardner, L. Kloo, L. Sun, *J. Am. Chem. Soc.* **2020**, *142*, 17681–17692.
- [20] R. A. Marcus, *Angew. Chem., Int. Ed.* **1993**, *32*, 1111–1121.
- [21] a) F. Würthner, *Chem. Commun.* **2004**, 1564–1579; b) Z. Yao, M. Zhang, R. Li, L. Yang, Y. Qiao, P. Wang, *Angew. Chem., Int. Ed.* **2015**, *54*, 5994–5998; *Angew. Chem.*, **2015**, *127*, 6092–6096.

- [22] N. E. Jackson, B. M. Savoie, K. L. Kohlstedt, M. Olvera de la Cruz, G. C. Schatz, L. X. Chen, M. A. Ratner, *J. Am. Chem. Soc.* **2013**, *135*, 10475–10483.
- [23] B. C. Lin, C. P. Cheng, Z. P. M. Lao, *J. Phys. Chem. A* **2003**, *107*, 5241–5251.
- [24] F. Panzer, H. Bässler, A. Köhler, *J. Phys. Chem. Lett.* **2017**, *8*, 114–125.
- [25] R. Steyrlleuthner, M. Schubert, I. Howard, B. Klaumünzer, K. Schilling, Z. Chen, P. Saalfrank, F. Laquai, A. Facchetti, D. Neher, *J. Am. Chem. Soc.* **2012**, *134*, 18303–18317.
- [26] P. Müller-Buschbaum, *Adv. Mater.* **2014**, *26*, 7692–7709.
- [27] Q. Zhang, M. A. Kelly, N. Bauer, W. You, *Acc. Chem. Res.* **2017**, *50*, 2401–2409.
- [28] J. F. Moulder, *Physical Electronics* **1995**, 230–232.
- [29] V. Gonzalez-Pedro, E. J. Juarez-Perez, W.-S. Arsyad, E. M. Barea, F. Fabregat-Santiago, I. Mora-Sero, J. Bisquert, *Nano Lett.* **2014**, *14*, 888–893.
- [30] F. Li, X. Deng, F. Qi, Z. Li, D. Liu, D. Shen, M. Qin, S. Wu, F. Lin, S.-H. Jang, J. Zhang, X. Lu, D. Lei, C.-S. Lee, Z. Zhu, A. K. Y. Jen, *J. Am. Chem. Soc.* **2020**, *142*, 20134–20142.

Entry for the Table of Contents



A polymeric hole-transport material (HTM) of **PC6** is delicately established, featuring a two dimensionally conjugated phenanthrocarbazole and S-O noncovalently conformational locking. Perovskite solar cells (PSCs) employing **PC6** as dopant-free HTM, afforded an excellent PCE of 22.2% and long-term stability, qualifying them as top-class PSCs based on dopant-free HTMs.